

In vivo three-dimensional microelectromechanical endoscopic swept source optical coherence tomography

Jianping Su,¹ Jun Zhang,² Linfeng Yu,² Zhongping Chen^{1,2}

¹Department of Biomedical Engineering, University of California, Irvine, Irvine, California 92612

²Beckman Laser Institute, University of California, Irvine, Irvine, California 92612

*Corresponding author: z2chen@uci.edu

Abstract: In clinical applications, three-dimensional (3-D) microscopic image volume reveals tissue morphological changes, which are closely related to pre-cancer and early stage disease, much better than two-dimensional images. However, the traditional endoscope only achieves two-dimensional surface images. In this paper, a 3-D endoscopic microscope was developed based on a rotational microelectromechanical system (MEMS) probe [1]. The 3-D helix scan mode was realized by combining a MEMS motor rotational scan and linear stage transversal movement. In order to coordinate the high spin speed of MEMS motor inside the endoscope, an optical coherence tomography (OCT) system with a broadband fast swept laser was used. *In vivo* 3-D image volumes of rabbit esophagus and trachea were demonstrated.

©2007 Optical Society of America

OCIS codes: (170.4500) Optical coherence tomography, (000.2170) Equipment and techniques.

References and links

1. P. H. Tran, D. S. Mukai, M. Brenner, and Z. Chen, "In vivo endoscopic optical coherence tomography by use of a rotational microelectromechanical system probe", *Opt.Lett.*, **29**, 1236-1238 (2004)
2. D. Huang, E. A. Swanson, C. P. Lin, J. S. Schuman, W. G. Stinson, W. Chang, M. R. Hee, T. Flotte, K. Gregory, C. A. Puliafito, J. G. Fujimoto, "Optical coherence tomography," *Science*, **254**, 1178-1181 (1991).
3. G. J. Tearney, S. A. Boppart, B. E. Bouma, M. E. Brezinski, N. J. Weissman, J. F. Southern, and J. G. Fujimoto, "Scanning single-mode fiber optic catheter-endoscope for optical coherence tomography", *Opt. Lett.* **21**, 543 (1996)
4. P. Herz, Y. Chen, A. Aguirre, J. Fujimoto, H. Mashimo, J. Schmitt, A. Koski, J. Goodnow, and C. Petersen, "Ultrahigh resolution optical biopsy with endoscopic optical coherence tomography", *Opt. Express*, **12**, 3532-3542 (2004)
5. S. H. Yun, G. J. Tearney, B. J. Vakoc, M. Shishkov, W. Y. Oh, A. E. Desjardins, M. J. Suter, R. C. Chan, J. A. Evans, I.-K. Jang, N. S. Nishioka, J. F. de Boer, and B. E. Bouma, "Comprehensive volumetric optical microscopy in vivo", *Nature Medicine*, **12**, 1429 - 1433 (2006)
6. S. Di Pietro, P. G. Arcidiacono, B. Mangiavillano, A. Mariani, P. A. Testoni, E. Masci, "Intraductal Optical Coherence Tomography for Investigating Main Pancreatic Duct Strictures", *Am J Gastroenterol.*, **102**, 269-274 (2007)
7. G. J. Tearney, B. E. Bouma, and J. G. Fujimoto, "High-speed phase- and group-delay scanning with a grating-based phase control delay line", *Opt. Lett.*, **22**, 1811-1813 (1997)
8. M. A. Choma, M. V. Sarunic, C. H. Yang, and J. A. Izatt, "Sensitivity advantage of swept source and Fourier domain optical coherence tomography," *Opt. Express*, **11**, 2183-2189 (2003)
9. S. H. Yun, G. J. Tearney, J. F. de Boer, N. Iftimia, and B. E. Bouma, "High-speed optical frequencydomain imaging," *Opt. Express*, **11**, 2953-2963 (2003)
10. J. Zhang, J. S. Nelson, and Z. P. Chen, "Removal of a mirror image and enhancement of the signal-to-noise ratio in Fourier-domain optical coherence tomography using an electro-optic phase modulator," *Opt. Lett.* **30**, 147-149 (2005)

11. R. Huber, M. Wojtkowski, and J. G. Fujimoto, "Fourier Domain Mode Locking (FDML): A new laser operating regime and applications for optical coherence tomography", *Opt. Express*, **14**, 3225-3237 (2006)
 12. B. Cense, N. Nassif, T. Chen, M. Pierce, S. -H. Yun, B. Park, B. Bouma, G. Tearney, and J. de Boer, "Ultrahigh-resolution high-speed retinal imaging using spectral-domain optical coherence tomography," *Opt. Express*, **12**, 2435-2447 (2004)
-

1. Introduction

Optical coherence tomography is a noninvasive, noncontact imaging modality that uses coherent gating to obtain high-resolution cross-sectional images of tissue microstructure [2]. Traditional OCT endoscope design uses a fixed gradient-index (GRIN) lens and prism as the optical tip. Rotational torque is transferred from the endoscope's proximal end to the distal tip [3-6]. In this design, the rotation of the whole endoscope, which is usually curved in the body, can cause unstable vibration and uneven rotational speed. This effect is more severe when the length of the endoscope increases. The rotational MEMS motor-based endoscope design eliminates this disadvantage by rotating only the optical tip of the endoscope. A prism mounted on the rotational MEMS motor reflects the focused beam out from the GRIN lens to create a circular scan. A high speed scan can be achieved by rotating a lightweight microprism with the MEMS motor. With the advantage of MEMS technology, the endoscope has a small diameter which is suitable for many clinical applications. Furthermore, this design can apply more flexible materials without the need of rotational torque transfer. Currently, our whole endoscope package diameter is 2.7 mm with a 2.2 mm MEMS motor inside. A longitudinal linear motor pulls the whole endoscope out slowly to create a 3-D helix scan.

2. Methods and materials

The schematic diagram of the endoscopic probe is shown in Fig. 1. The distal end was enclosed by round-shaped medical ultraviolet glue to reduce tissue damage when the probe was advanced into the internal organ. Inside the biocompatible fluorinated ethylene-propylene (FEP) tube, a MEMS motor with a diameter of 2.2 mm was backward mounted at the distal end of the probe and was driven by the outside motor controller through a control wire. The 1310 nm single mode fiber was cut to 8 degrees and glued to a focusing GRIN lens. The focused beam was reflected by a right angle microprism which was glued to the motor shaft toward the sample. The only rigid part from the optical glue point to the round-shaped end was 2.5 cm long. The diameter of the whole endoscope package was 2.2 mm. Compared to our previous design of a rotational MEMS probe [1], the motor no-load rotation speed limit of the current design increases 20% but at the cost of an increase in size of 15 %. The motor rotation in the current design is much more stable through the cycle feedback control, which is critical for synchronization in 3-D slice image acquisition. In addition, the MEMS motor is more robust with an outside steel sheath which strengthens the connection between the gear head and rotational shaft. The endoscope was fixed to a linear transversal scan stage at the proper point. To create a 3-D helix scan, the whole probe was pulled back slowly by a linear scan stage while the prism was rotated rapidly by the MEMS motor.

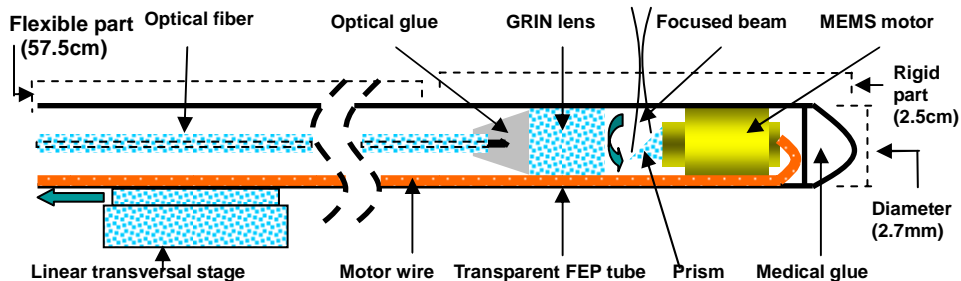


Fig. 1. Schematic of 3-D MEMS motor-based endoscope.

Figure 2 shows serial photos of the endoscope in 3-D working mode. The major advantage of the MEMS motor-based endoscope was that coupling rotation torque from the proximal end of the traditional endoscope was not necessary. The aluminum-coated prism was the sole moving part in achieving a 360 degree full circle view. Because the microprism was lightweight, the real time frame rate (30 frames/second) could be achieved easily by the MEMS motor's output torque. Since the whole endoscope rotation was eliminated, the metal sheath of a traditional endoscope for reinforcement was not needed. Hence, endoscope flexibility increased. In addition, the fiber rotator joint between the traditional rotational endoscope and static sample arm fiber was discarded, which decreased coupling power fluctuation.

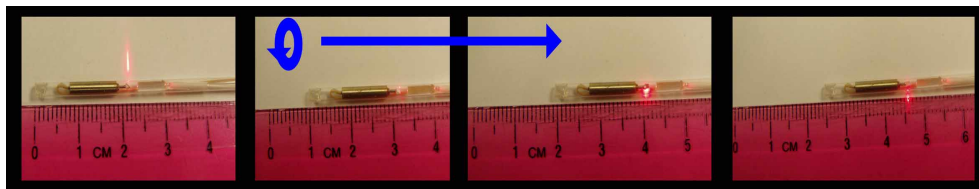


Fig. 2. Endoscope in 3-D working mode. The whole endoscope moves from left to right. The red dots indicate the output beam orientation reflected by the microprism.

Traditional time domain OCT can only realize an A-scan rate of less than a few KHz by using a mechanical depth scanning optical delay line. Thus, it is not suitable for 3-D imaging [7]. Swept source OCT which is based on Fourier domain technique can achieve a 10 to 100 times increase in imaging speed compared to the time domain OCT technique with enough SNR for *in vivo* clinical applications [8-11]. The high imaging speed of swept source OCT enables us to map real time 3-D imaging with better identification of multiple lesions and superior mapping of lesion margins than 2-D imaging.

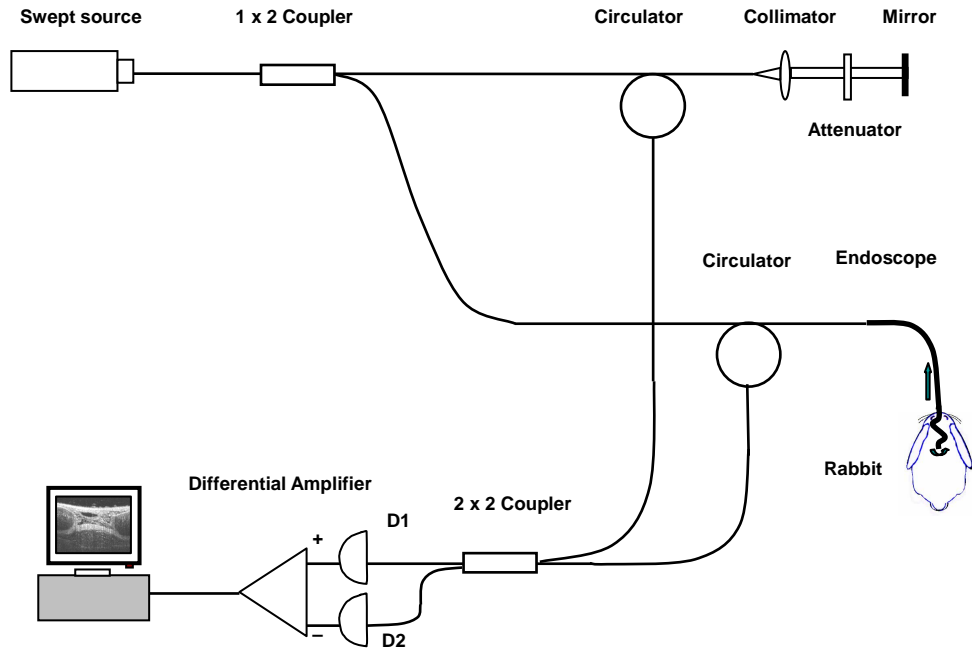


Fig. 3. The fiber-based swept source OCT system setup: fixed mirror and attenuator work as the reference arm; MEMS motor rotates the microprism inside the endoscope while the outside stage pulls the whole endoscope. Balanced detection is used to increase SNR.

The schematic diagram of the fiber-based swept source OCT system is shown in Fig. 3. The output light from a swept light source (Santec Corporation, Komaki, Aichi, Japan) at 1310 nm with a FWHM bandwidth of 100 nm and output power of 5 mW was split into reference and sample arms by a 1×2 coupler. The light source was operated at a sweeping rate of 20,000 Hz. Eighty percent of the incident power was coupled into the sample arm while 20% was fed into the reference arm. The reference power was attenuated by an adjustable neutral density attenuator for maximum sensitivity. The MEMS motor-based endoscope was connected to the sample arm. The flexibility of the endoscope enabled its access into the internal organ easily. Two circulators were used in both reference and sample arms to redirect the back-reflected light to a 2×2 fiber coupler (50/50 split ratio) for balanced detection. In the detection arm, the time fringe signal collected by the photodetectors was digitized by a 14 bit data acquisition board (National Instrument high speed digitizer 5122) sampling at 33 M samples/s, and the number of data points for each A-line data acquisition was 1024. The swept source generated an A-line trigger signal that was used to initiate the data acquisition process for each A-line. The complex analytical depth encoded signal was converted from the collected time fringe signal by fast Fourier transform. The structure image was reconstructed from the amplitude term of the complex depth encoded signal. The measured axial resolution of $8 \mu\text{m}$ was close to the theoretical axial resolution of $7.5 \mu\text{m}$ since the spectrum of the swept light source is nearly Gaussian shaped. The lateral resolution, which is determined by the endoscope's focus spot, was measured to be $20 \mu\text{m}$ with a beam profiler. The measured sensitivity of the OCT system with an ideal partial reflector as the sample was 108 dB. The endoscope's one way loss was measured to be only 1 dB owed to the MEMS motor-based design. Thus, the signal-to-noise ratio of the OCT system with the probe was 106 dB. To cancel the dispersion generated by the endoscope optics, a software dispersion compensation algorithm was applied [12]. By use of a mirror as the sample object, the dispersive phase term was measured and averaged from 500 continuous A-lines. The

dispersion was cancelled by subtracting the calibrated dispersive phase term from the phase term of the complex depth encoded signal.

3. Results and conclusion

In vivo rabbit trachea and esophagus were imaged in 3-D mode. Four thousand A-lines were taken for one frame. At the A-line rate of 20 KHz, the scan time for one frame was 0.2 second. The MEMS motor was driven at a rotating speed of 5 circles/sec to be synchronized with the B-scan. Due to data transfer and processing delays, the data acquisition board was paused for 0.8 second after the acquisition for every B-scan. Thus, the overall image display rate was 1 frame/sec. The linear motor was scanned at 10 $\mu\text{m}/\text{sec}$. A total of 600 image slices were recorded to rebuild 3-D volume with a length of 6 mm. The longitudinal cross-sectional image could be reconstructed from 3-D image volume.

The tissues were immediately fixed after taking OCT images in a phosphate buffered (pH 7.6) 10% formalin solution for 24 hours and then rinsed in a phosphate buffer. After dehydration in progressive concentrations of ethanol-water, the tissues were cleared with HistoClear (National Diagnostics, Manville, NJ) and infiltrated with paraffin in a tissue processor (Triangle Biomedical Sciences ATP-1). The tissues were then embedded vertically in paraffin. Six micrometers serial sections were cut through the OCT imaging zone and carefully placed on a clean glass slide. The sections were deparaffinized with HistoClear, stained in hematoxylin and eosin, and coverslipped. Histology photos were taken from these sections. Figure 4(a) shows the 3-D volume image of *in vivo* rabbit esophagus. Figure 4(b) is one of the recorded cross-sectional images sliced from the 3-D volume. The 9.86 mm by 1.85 mm transversal slice unwrapped from Fig. 4(b) is shown in Fig. 4(c). The histological result at the corresponding location of Fig. 4(c) is shown in Fig. 4(d). From the unwrapped transversal slice, the layer epithelium, lamina propria, muscularis mucosae, submucosa and muscularis externa are obvious and match well with the histological result.

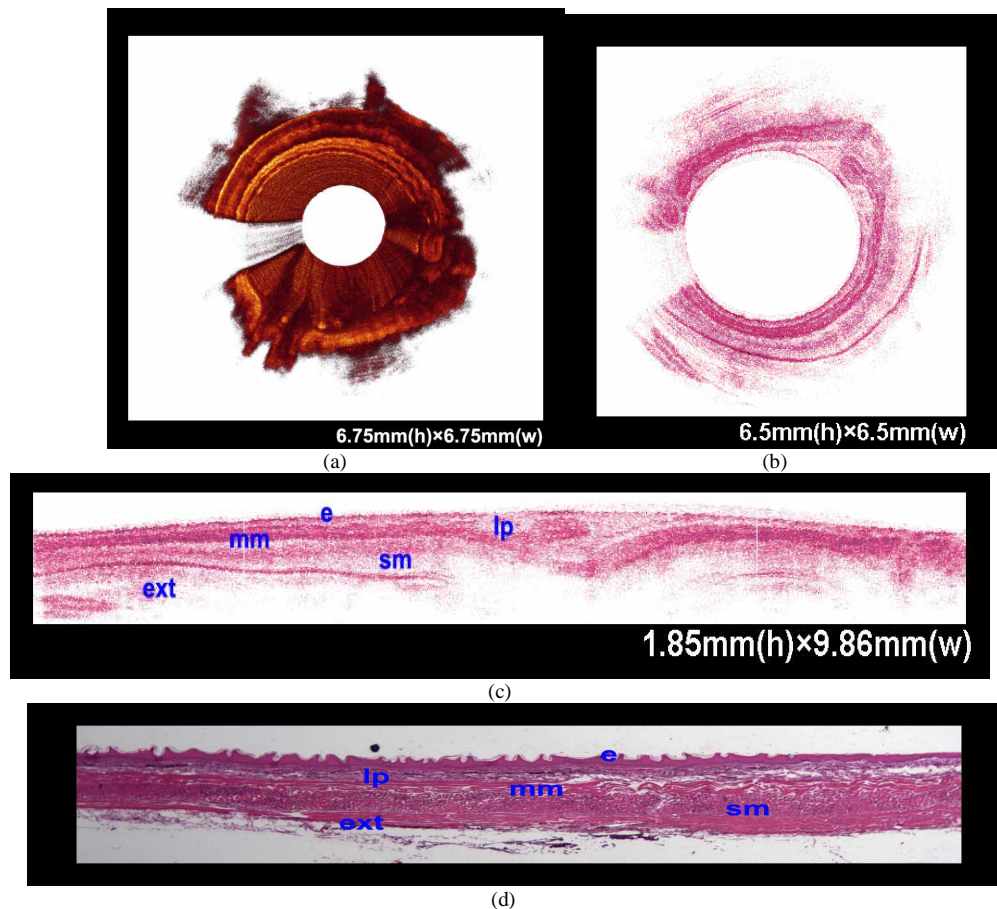


Fig. 4. (a) Three-dimensional rebuilt image of rabbit esophagus which was 6 mm long; the movie shows the different angle of the three-dimensional rebuilt volume. (b) One cross-sectional slice pulled out from (a); the movie shows the whole slices set sequentially. (c) The transversal image unwrapped from (b) whose size was 9.86 mm by 1.85 mm. (d) The histology image at corresponding position of (c). (e=epithelium; lp=lamina propria; mm=muscularis mucosae; sm=submucosa; ext=muscularis externa.)

Figure 5(a) shows an *in vivo* rabbit trachea 3-D volume image. The surrounding trachea ring is clearly visible in the middle part; Fig. 5(b) is one of the recorded cross-sectional images sliced from the 3-D volume. The light color ring in the margin part is the rotational cross-section view of the trachea ring. The reconstructed longitudinal slice between arrow points in Fig. 5(a) is shown in Fig. 5(c); the transversal cross-section trachea ring can be seen in the lower part. Figure 5(d) is the histology image at the corresponding location of Fig. 5(c). From the reconstructed longitudinal slice figure, the layer epithelium, lamina propria, submucosa, cartilage and trachealis muscle are visible.

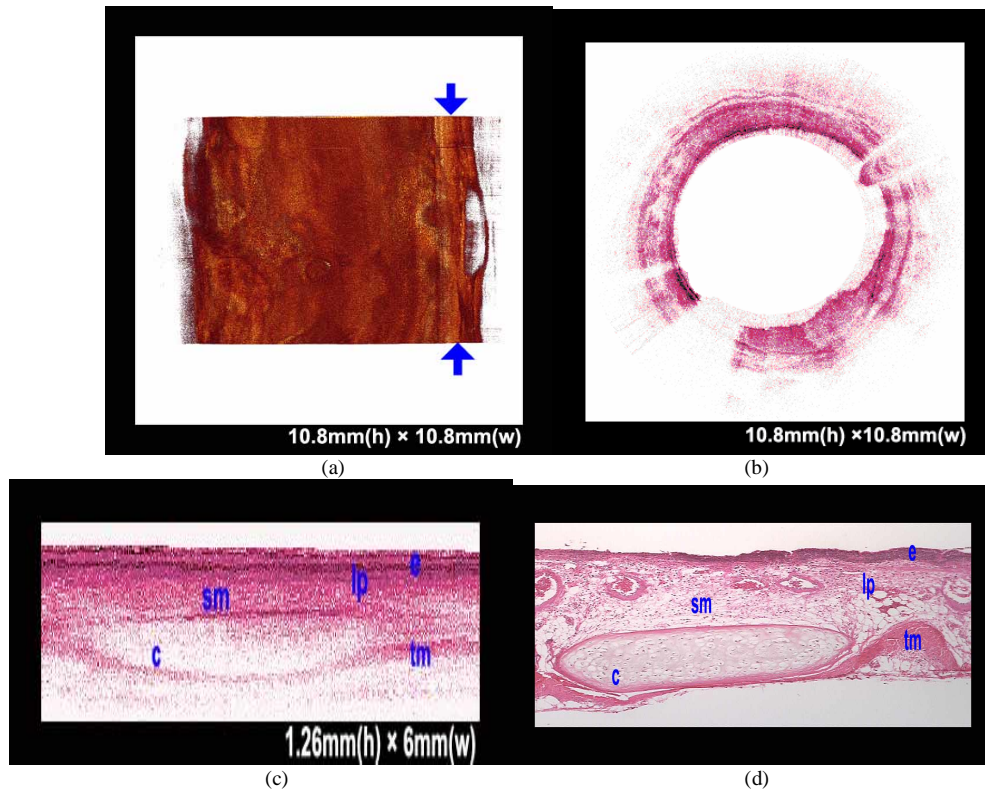


Fig. 5. (a) Three-dimensional rebuilt image of rabbit trachea which was 6 mm long; the trachea ring is visible in the middle part. (b) One cross-sectional slice pulled out from (a); the movie shows the whole slices set sequentially. (c) A longitudinal cross-sectional image rebuilt from 3-D image volume; the image size was 6 mm by 1.3 mm. (d) The histology image at corresponding position of (c). (e=epithelium; lp=lamina propria; c=cartilage; sm=submucosa; tm= trachealis muscle.)

In summary, a MEMS motor-based 3-D scanning endoscopic probe was developed. High resolution and high speed microscopic image acquisition was achieved by integrating the endoscopic probe with a high speed swept source OCT system. *In vivo* 3-D imaging of rabbit esophagus and trachea was demonstrated. This design is also suitable for imaging other internal organ tissues such as gastrointestinal tract, airway, urethral tract and blood vessel.

Acknowledgments

This work was supported by research grants from the National Science Foundation (BES-86924), National Institutes of Health (EB-00293, NCI-91717, RR-01192), Air Force Office of Scientific Research (FA9550-04-1-0101), and the Beckman Laser Institute Endowment.